DOI: 10.1021/cg1015093

CRYSTAL GROWTH & DESIGN Article

2011, Vol. 11
594–599

Promotional Effects of Bismuth on the Formation of Platinum−Bismuth Nanowires Network and the Electrocatalytic Activity toward Ethanol Oxidation

Wenxin Du, Dong Su, Qi Wang, Anatoly I. Frenkel, and Xiaowei Teng*

Department of Chemical Engineering, University of New Hampshire, Durham, New Hampshire 03824, United States, Center for Functional Nanomaterials, Brookhaven National Laboratory, Upton, New York 11973, United States, and Department of Physics, Yeshiva University, New York, New York 10016, United States

Received November 11, 2010; Revised Manuscript Received December 16, 2010

ABSTRACT: Electrocatalytic activities of Pt and their alloys toward small organic molecules oxidation are highly dependent on their morphology, chemical composition, and electronic structure. Here, we report the synthesis of dendrite-like $Pt_{95}Bi_5$, $Pt_{83}Bi_{17}$, and $Pt_{76}Bi_{24}$ nanowires network with a high aspect ratio (up to 68). The electronic structure and heterogeneous crystalline structure have been studied using combined techniques, including aberration-corrected scanning transmission electron microscopy (STEM) and X-ray absorption near-edge structure (XANES) spectroscopy. Bismuth-oriented attachment growth mechanism has been proposed for the anisotropic growth of Pt/Bi. The electrochemical activities of Pt/Bi nanowires network toward ethanol oxidations have been tested. In particular, the as-made $Pt_{95}Bi_5$ appears to have superior activity toward ethanol oxidation in comparison with the commercial Pt/C catalyst. The reported promotional effect of Bi on the formation of Pt/Bi and electrochemical activities will be important to design effective catalysts for ethanol fuel cell application.

Introduction

In the last few decades, there has been a growing interest in direct electrocatalytic conversion of small organic molecules (SOMs) into electrical energy by the so-called direct fuel cell reaction, which holds great promise for future green technology for various applications, especially in portable electronics.[1−4] As one of the most studied SOMs fuel cell reactions, the direct methanol fuel cell (DMFC), involving six-electron transfer methanol oxidation, directly utilizes liquid methanol fuel to deliver continuous power with higher utilization efficiencies and lower emission of pollutants, in sharp contrast to conventional internal combustion engines.[5−9] On the other hand, ethanol emerges as another SOM with several advantages in fuel cell technology compared with methanol. First, ethanol is safer (the fatal dose for an adult is over 500 mL); second, ethanol has a relatively higher boiling point (78 °C), making it easier to store and transport than methanol; third, ethanol has more energy density (∼8 kwh/kg) than methanol (∼6 kwh/kg) due to the nature of a twelve-electron transfer upon complete oxidation;[3,4] fourth, ethanol is more easily available from renewable sources.[10,11] Therefore, ethanol becomes the ideal combustible for low-temperature fuel cell reactions. The major impediment to the full-scale commercial production of direct ethanol fuel cell (DEFC) stacks is the activity and cost of electrocatalysts. Pt-containing alloy catalyst, PtRu in particular, has been employed as the one of the most effective anode catalysts because of its excellent performance in the dehydrogenation of SOMs and higher tolerance to CO poisoning compared with pure Pt.[12−17] In addition, PtBi has also attracted great research interest.[18−24] For example, both bulk and nanosized (10−19 nm) Pt/Bi materials exhibited superior electrocatalytic activity toward various SOMs oxidation and showed great CO tolerance.[25−30] However, the synthesis of monodispersed Pt/Bi electrocatalysts with an average size of less than 3−4 nm, which is the more favorable size range for actual fuel cells, has not been well studied to date.

Previous experiments of electrooxidation of SOMs on single crystals have also indicated that the catalytic activity of Pt and its alloyed nanomaterials is highly dependent on their morphology.[31−36] The synthesis and study of electrochemical activity of cubes, truncated cubes, dendrites, and hollow structures have been intensively studied.[31,37−42] The one dimensional (1D) Pt-containing nanostructure has also attracted special interest, although synthetic challenges in the fine control over morphology arise from unfavorable anisotropic growth of symmetric cubic lattice structures.[33,43,44] The synthesis of 1D Pt/Bi ultrathin nanowires (NWs) network and the investigation of their electrocatalytic behavior have, to our knowledge, not been reported to date. Herein, we report the synthesis and electrochemical activities toward ethanol oxidations of an as-made ultrathin dendrite-like Pt/Bi NWs network with an average width of less than 3.6 nm. The crystalline and electronic structures of Pt/Bi have been investigated by advanced aberration-corrected scanning transmission electron microscope (STEM) equipped with electron energy loss spectrometer (EELS), and X-ray absorption near-edge structure (XANES) spectroscopy. Our results unambiguously indicate the Bi-orientated attachment growth of the Pt/Bi NWs network and the promotional effect of Bi on the oxidation of ethanol.

Experimental Section

Synthesis of PtBi NWs Network. In a typical synthesis of $Pt_{95}Bi_5$ nanowires network, ethylene glycol (8 mL, Alfa Aesar, 99%) and polyvinylpyrrolidone (PVP) (55 mg, Acros, MW = 58 000) were mixed in a three-neck flask and heated to 170 °C using an oil bath

*To whom correspondence should be addressed. Tel: 603-862-4245. Fax: 603-862-3747. E-mail: xw.teng@unh.edu.

 Published on Web 01/11/2011

under argon protection. Then, the fresh-made mixture of Na_2PtCl_4 (32 mg, 0.07 mmol, Alfa Aesar, 99.95%), $Bi(NO_3)_3 \cdot 5H_2O$ (3.6 mg, 0.007 mmol, Alfa Aesar, 98%), and ethylene glycol (3 mL, AR, Mallinckrodt Chemicals) was injected into the flask. The solution was kept at 170 °C for 10 min before being cooled to room temperature. The product was washed thoroughly with ethanol and acetone to remove ethylene glycol and excess PVP. For the synthesis of other Pt/Bi nanowires networks, only the amount of the precursors changed. For example, the amount of Na_2PtCl_4 and $Bi(NO_3)_3$ was 33.4 mg and 12.3 mg for the synthesis of the $Pt_{83}Bi_{17}$ nanowires network, while 18.3 mg and 20.4 mg for the synthesis of the $Pt_{76}Bi_{24}$ nanowires network.

STEM and EELS Characterizations. The STEM and EELS measurements were performed at the Center for Functional Nanomaterials, Brookhaven National Laboratory (USA). The dedicated aberration-corrected STEM, Hitachi HD 2700C, operated at 200 kV, was equipped with a modified Gatan Enfina ER spectrometer. The probe size was around 0.8−1.3 Å and the electron beam intensity on the sample varied from 100 to 200 pA depending on the tuning conditions of the microscope. The cold field emission gun gave an energy resolution of 0.35 eV as measured from the full width at half maximum (FWHM) of the zero-loss peak. The convergence angle was 27 mrad and the ADF and EELS collection angles were 45−242 and 20 mrad, respectively. For acquiring the EELS, the dwelling time for each pixel was about 10 s. Comparison between the images taken before and after analysis showed no discernible change in the sample caused by beam damage. Regular transmission electron microscopy (TEM) measurements were performed at the University of New Hampshire using a Zeiss/LEO 922 Omega TEM. Image acquisition and analysis were performed using Gatan Digital Micrograph and ImageJ software. The standard deviation was calculated by averaging at least 120 measurements.

XANES Characterization. XANES was performed at beamlines X18B at the National Synchrotron Light Source (NSLS), Brookhaven National Laboratory, Upton, New York. The storage ring energy was 2.5 GeV, and the ring current was in the range of 110−300 mA. A double-crystal Si (111) monochromator was used to scan X-ray energy from −150 to 1330 eV relative to Pt L3 edge (11 564 eV) and from −150 to 1330 eV relative to Bi L1 edge (16 388 eV). PtBi NWs network samples (~30 mg) were prepared by drop-casting concentrated nanomaterials solution onto Kapton tape evenly for adequate uniformity for XAFS measurements. Standard metal (Bi and Pt) foils were placed between the transmission and reference X-ray detectors and measured simultaneously with all the nanomaterials samples, for X-ray energy calibration and data alignment. Data processing and analysis were performed using the IFEFFIT package. IFEFFIT is a specialized program for X-ray absorption data analysis. It combines the high-quality analysis algorithms with graphical display of data and general data manipulation. IFEFFIT is under active development but is fairly well tested and ready for use.

Electrochemical Measurements. The electrochemical properties were examined with a CHI 660 single channel electrochemical workstation (CH instruments, Inc.) The three-electrode system comprises a glassy carbon rotating disk electrode (RDE, 5 mm in diameter, Pine Research Instrumentation) as working electrode, a thin platinum wire as counter electrode, and a Ag/AgCl (1 M KCl) electrode as reference electrode. The water dispersions of the Pt/Bi NWs network and Pt/C (E-TEK, 60 wt % Pt) were used as catalysts. The typical loading of catalyst was 3−5 μg of total metal. All the catalysts were suspended in the 10 μL of deionized water and well sonicated before drop-casting on the glassy carbon electrode surface. Because of the surface tension of aqueous solution, the catalyst suspension was constrained within the boundary of the glassy carbon electrode. The droplets of catalysts were dried in a fume hood, followed by covering with 10 μL of diluted Nafion solutions (0.5% V/V). Finally, the catalysts formed a uniform assembly upon the evaporation of solvents. The cyclic voltammograms (CV) curves were recorded from −0.3 to 1.2 V in 0.1 M argon-purged perchloric acid ($HClO_4$, 70%, Alfa Aesar) solution to measure the hydrogen adsorption/desorption behavior. CV curves of those as-made catalysts toward the alcohol oxidation were recorded in 0.1 M $HClO_4$/0.125 M ethanol solution between −0.2 to 1.2 V under argon-purged environment. The potential sweep rate was 60 mV/s. Chronoamperometry (IT) was carried out at a potential of 0.55 V for 1.5 h right after completion of CV measurements. All electrochemical measurements were carried out at room temperature. Dissolved oxygen was removed from the solution by bubbling argon for 40 min prior to the measurement.

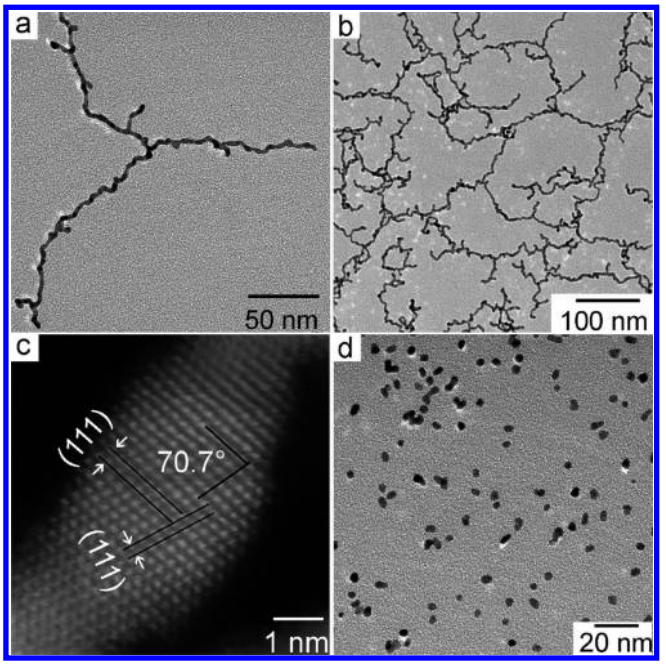

Figure 1. TEM images of as-made (a−c) $Pt_{95}Bi_5$ NW networks and (d) Pt nanoparticles made without the addition of $Bi(NO_3)_3$.

Results and Discussion

Pt/Bi NWs networks were synthesized via the Polyol process by simultaneous reduction of sodium tetrachloroplatinate (Na_2PtCl_4) and bismuth nitrate ($Bi(NO_3)_3 \cdot 5H_2O$) at 170 °C under an inert atmosphere. The ethylene glycol was used as both a solvent and reducing agent, and PVP was used as a capping agent. Figure 1 shows the TEM images of the as-made Pt/Bi dendrite-like NWs network synthesized by a molar ratio of Pt/Bi around 10:1. Those networks have an average length of 245 ± 81 nm (calculated from the longest branches) and width of 3.6 ± 0.5 nm, which led to an average aspect ratio of ~68. The chemical composition of Pt/Bi was analyzed by energy dispersive X-ray spectroscopy (EDS) for a NWs network assembly which covered an area of 1 μm^2. The EDS spectrum showed an average composition of $Pt_{95\pm0.8}Bi_{5.0\pm0.8}$ from six randomly picked areas (Figure S1, Supporting Information). A state-of-the-art cold field emission Hitachi HD-2700C STEM with an aberration-corrector was further used to study the crystalline structure of an individual NW network (Figure 1c). At present, the aberration-corrected STEM has been revolutionizing its performance, by dramatically improving spatial resolution and the beam current at a given resolution by a few more orders of magnification.[45,46] In this context, it could claim to be the most precise instrument ever constructed, exhibiting a strong ability to analyze materials with a resolution of a single atom, which provides great opportunities to interpret the real structure of individual nanomaterials. Figure 1c shows an atomic resolution high angle annular dark field (HAADF) image taken with STEM. The lattice distance normal to the growth direction of the nanowires network was calculated to be 2.4 Å,

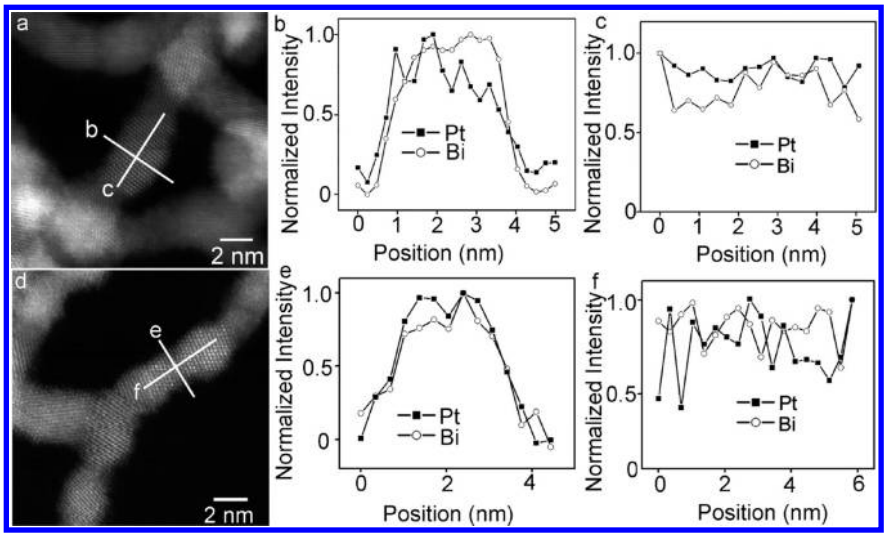

Figure 2. (a, d) HAADF images of (a−c) $Pt_{95}Bi_5$ and (d−f) $Pt_{83}Bi_{17}$ NW networks. And the EELS line scans (b, e) across and (c, f) along the individual Pt/Bi NW.

which could be assigned to the {111} planes of $Pt_{95}Bi_5$. The high-resolution TEM (HRTEM) image also shows the well-resolved lattice planes at a 71° angle to the {111} plane had a d-spacing of 2.4 Å, which could also be assigned to the {111} plane of face centered cubic (fcc) phase Pt/Bi alloys. Our results show that Bi appears to be the key for successful growth of the Pt/Bi NWs network. In the absence of Bi, only faceted Pt nanoparticles were produced (Figure 1d).

By varying the molar ratio of Na_2PtCl_4 and $Bi(NO_3)_3$ from 10:1 to 3:1, and 1:1, $Pt_{83}Bi_{17}$ and $Pt_{76}Bi_{24}$ NWs networks were also synthesized, respectively (Figure S2, Supporting Information). $Pt_{83}Bi_{17}$ and $Pt_{76}Bi_{24}$ NWs networks have an average width of 2.7 ± 0.4 and 3.6 ± 0.6 nm. Although those NWs netwroks are very similar in 1D morphology as TEM indicated, when the Bi content is very low, for example, 5% and 17%, the formed products were rather smooth. On the other hand, when the Bi content increases to 24%, the NWs networks present a pearl-necklace appearance. We noticed that when the Bi content increased to 67%, aggregated particles were formed (Figure S3, Supporting Information).

We further used electron energy loss spectroscopy (EELS) to investigate the atomic distribution of Pt and Bi within the NW simultaneously. In particular, the EELS equipped at the aberration-corrected STEM can routinely achieve an energy resolution of 0.35 V at zero energy loss, allowing selective analysis of Pt and Bi in the NW separately by choosing proper energy values based upon the atomic absorption of electrons during electron−electron interaction. Therefore, the distribution of heterogeneous atoms of the individual NW with atomic resolution can be determined. Figure 2 shows the intensity profiles of Pt and Bi acquired from M edges of $Pt_{95}Bi_5$ and $Pt_{83}Bi_{17}$ NWs networks. Line scans along and across the nanowires network demonstrate the coexistence of Pt and Bi. Moreover, steady signal intensity along both directions further demonstrates the homogeneous mixing of Pt and Bi within the entire NW network, confirming the random alloying between Pt and Bi inside the NW networks.

To explore the growth mechanism of Pt/Bi NWs network, we systematically analyzed the growth kinetics by examining the intermediate products during the formation of $Pt_{95}Bi_5$ (Figure 3). TEM images show the formation of $Pt_{95}Bi_5$ as the reaction time ranged from 1 to 120 min, after injection of precursor mixture into preheated ethylene glycol solution (170 °C) in the presence of PVP. Nearly spherical nanocrystals with an average diameter of 3.1 ± 0.4 nm began to appear at 1 min after injection. The concentration of product nevertheless was rather low at this stage. These nanocrystals grew rapidly into a short nanorod at 3 min with an average width of 2.8 ± 0.5 nm, and a length of 9.7 ± 3.6 nm. Most of the precursor was reduced at this stage, evidenced by the rapid change of solution color from brownish to black. Elongated nanorods were formed at 5 min with similar width (3.1 ± 0.4 nm) but increased length (26.3 ± 16.3 nm). The NWs networks with the high aspect ratio (~68) formed after 10 min reaction with an average length of 245 ± 81 nm and width of 3.6 ± 0.5 nm. Note that even after 120 min reaction, Pt/Bi still maintained a NW network morphology. The preferential growth of the Pt/Bi NWs network along the axial (as shown in Figures 1c and 2a) instead of the radial direction strongly indicated a head−head attachment anisotropic growth mode.[47,48]

The anisotropic growth of cubic Pt and its alloy is rather unexpected owing to an apparent lack of crystal lattice asymmetry.[49−53] Here we proposed a bismuth-oriented growth for the formation of the Pt/Bi nanowires network (Figure 4). Since the standard reduction potential of Pt^{2+} (1.20 V vs standard hydrogen electrode (SHE)) is higher than that of Bi^{3+} ions (0.32 V), Pt-rich atoms core formed first during the reduction, followed by sequential growth of Bi on the surface of Pt seeds. Bi-shell-rich Pt/Bi embryonic nanostructures will be further connected preferentially via asymmetric rhombohedral Bi lattice, resulting in the anisotropic growth of the Pt/Bi NWs network. The promotional effect of Bi on the anisotropic growth of Pt/Bi can also be evidenced by the fact that only faceted Pt nanoparticles were formed without the addition of a Bi precursor under the identical experimental conditions (Figure 1d).

We next studied the electronic structure of the Pt/Bi nanowires network using XANES. As an element-specific charge state probe, XANES is ideally suited to study the electronic structure by comparing the changes in the intensity of the white lines (intense peaks at the L absorption edges) from both the Pt and Bi.[54−56] Figure 5 plots the normalized XANES spectra from the Pt L_3 and Bi L_1 edges of Pt/Bi NWs network

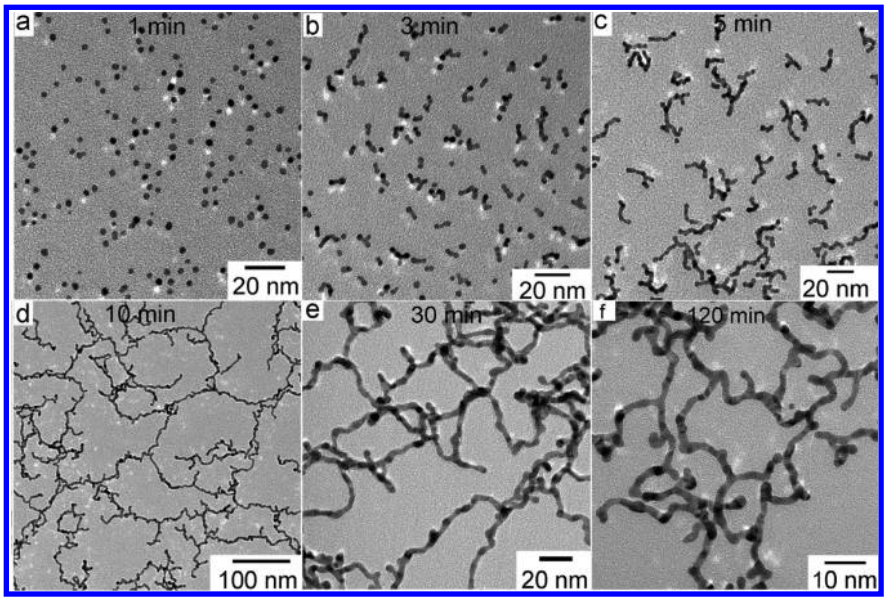

Figure 3. TEM images of $Pt_{95}Bi_5$ NW networks synthesized at a reaction time of (a) 1 min, (b) 3 min, (c) 5 min, (d) 10 min, (e) 30 min, and (f) 120 min.

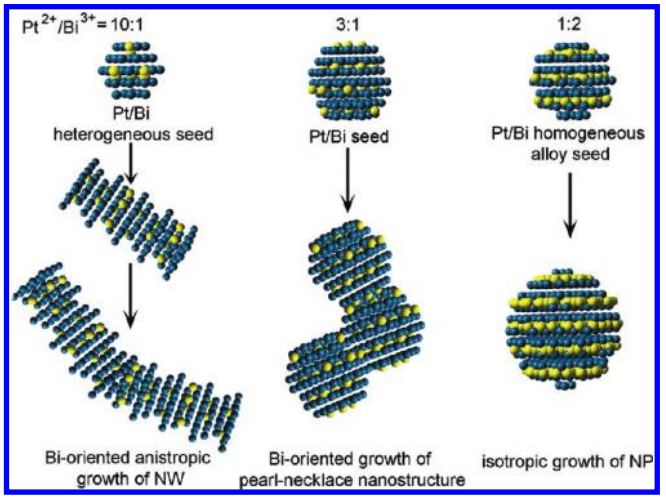

Figure 4. Schematic drawing of Bi-oriented growth of Pt/Bi nanomaterials with stoichiometry-dependency (Bi: yellow, Pt: blue).

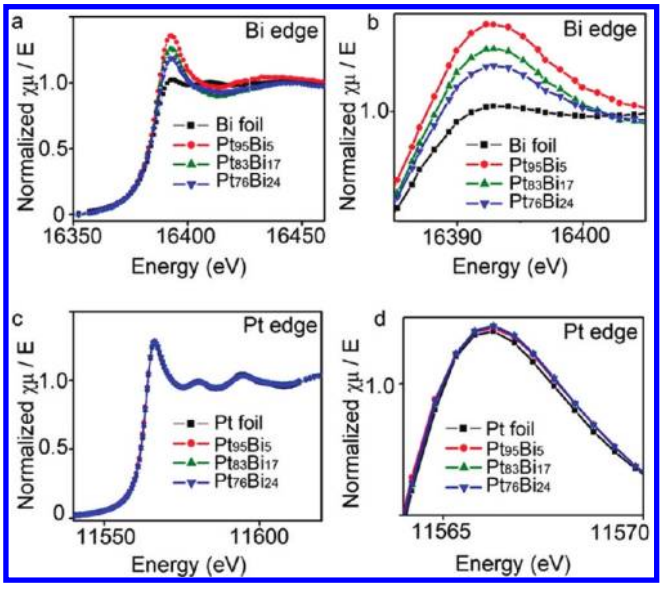

Figure 5. XANES spectrum of (a, b) Bi L_1 edge and (c, d) Pt L_3 edge of as-made $Pt_{95}Bi_5$, $Pt_{84}Bi_{16}$, and $Pt_{76}Bi_{24}$ NW networks, as well as Pt foil and Bi foil as references.

and those from Pt and Bi foils as references. It shows that the intensities of the Bi white line feature are noticeably higher than that of the pure Bi foil. Since the white line features in the Bi L_1 edge arise from 2s to 6p dipole transitions, these observations point to an increase in the number of unoccupied states of p character at the Bi site in the Pt/Bi nanowires network.[57] The increased Bi white line intensity in the Pt/Bi NWs network could be attributed to Bi oxidation, owing to the high vulnerability of Bi metal to oxygen. In fact, the oxidation of Bi has also been reported in the ordered intermetallic PtBi bulk materials at room temperature.[29] The possibility of the enhanced Bi white line intensity was mainly because of the charge transfer from Bi atoms to Pt atoms can be excluded, since the Pt L_3 white lines of Pt/Bi NWs network actually increase slightly relative to the Pt foil. In this context, white line intensities of Pt would be expected to decrease relative to Pt foil if charges transferred from Bi to Pt sites. It is also interesting to point out that the white line intensity of the Bi L edge increases as the Bi concentration decreases, indicating that $Pt_{95}Bi_5$ NWs network was the most oxidized and $Pt_{76}Bi_{24}$ NWs network was the least oxidized. The stoichiometry-dependent oxidation state of various Pt/Bi NWs networks might indicate that the Bi atoms located in the core region of $Pt_{83}Bi_{17}$ and $Pt_{76}Bi_{24}$ NWs network were not as completely oxidized as those in the $Pt_{95}Bi_5$ NWs network were.

The electrocatalytic activities of the Pt/Bi NWs network and commercial Pt/C catalysts on the ethanol oxidation reactions were further measured in the CV measurements (Figure 6). During the forward scan, the oxidation of ethanol gives two anodic current peaks at ~0.6 V and ~1.0 V, respectively. The highest ethanol oxidation current density at 0.588 V was obtained with Pt/C, and $Pt_{83}Bi_{17}$ showed the least current density. Not surprisingly, addition of Bi will lead to the negative shift of peak potential as observed in the case of methanol oxidation. Although $Pt_{95}Bi_5$ showed lower current density compared to the commercial Pt/C catalyst in CV

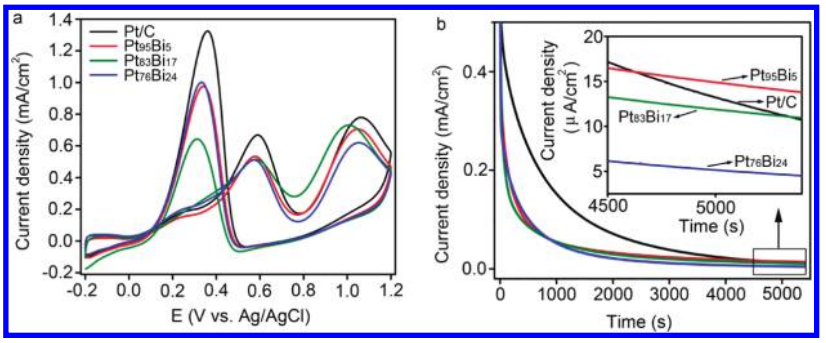

Figure 6. (a) Cyclic voltammograms and (b) chronoamperometric measurements of Pt/Bi NW networks and Pt/C for the oxidation of ethanol.

measurements, it appeared the better performance in the IT measurements performed at 0.55 V for 1.5 h (Figure 6b). The current density of $Pt_{95}Bi_5$ NWs network after 1.5 h operation showed a higher steady-state current density (13.8 μA cm^{-2}) compared with that of Pt/C (10.7 μA cm^{-2}), while $Pt_{83}Bi_{17}$ NWs network showed very similar current density as Pt/C after 1.5 h reaction (10.9 μA cm^{-2}). We noticed the ethanol concentration was 0.125 M with a volume of 100 mL; during the electrochemical measurement, molar fractions of reacted ethanol for Pt/C and $Pt_{95}Bi_5$ were estimated to be less than 0.1%. Therefore, a higher steady current density with $Pt_{95}Bi_5$ compared to Pt/C in the IT measurements did not result from the difference in ethanol concentration, even though Pt consumed more ethanol than $Pt_{95}Bi_5$ in the early stage.

Previous results on single crystals demonstrated that transition metal atoms including Bi exhibited opposing modes of actions on the Pt surface.[19,20] On the one hand, Bi gave an inhibiting effect due to blocking active Pt sites for SOMs adsorptions; on the other hand, it showed a promotional effect due to enhanced adsorption of water on Pt sites adjacent to Bi atoms, and consequently an increased rate of SOMs oxidation by generating oxygenated species (e.g., adsorbed OH from water). In the case of ethanol oxidation, the enhancement role of Bi is dominant, evidenced by improved activities of $Pt_{95}Bi_5$ and $Pt_{83}Bi_{17}$ NWs networks in IT measurements. It is well-known that electro-oxidation of ethanol is more complicated than that of methanol, since more intermediates would be generated during the oxidation of ethanol, such as CO, acetaldehyde, and acetic acid.[58−61] Therefore, the ability of oxidizing intermediates appears more important in the catalyst design for ethanol oxidation. Better catalytic activity of Pt/Bi NW networks on ethanol oxidation was attributed not only to the electronic structure modification of the Pt surface with the presence of Bi but also oxygenated species from the interaction between Bi and water. This can be further confirmed by XANES analysis, by which Bi exists as an oxide and/or hydroxide in the Pt/Bi NW networks. These oxygenated species may contribute to the oxidation of dissociated acetaldehyde (into acetic acid) or possible CO (into CO_2), rendering Pt/Bi NW networks as a "bi-functional" catalyst for the ethanol oxidation. More interestingly, the rival action of Bi showed that the activity over ethanol oxidation is also highly dependent on the stoichiometry as our current research indicated, showing that $Pt_{95}Bi_5$ NW networks appeared the most active. It indicated that 5% Bi might be the optimized concentration in Pt/Bi by balancing well the surface concentration of Pt atoms and the oxygenated species.

Although the nature of ethanol oxidation at both anodic peak potentials is unclear, it has been speculated that neither Pt/Bi nor Pt would oxidize ethanol completely to CO_2. The

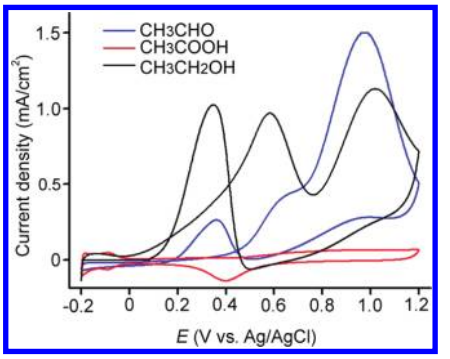

Figure 7. Cyclic voltammograms of $Pt_{95}Bi_5$ NW networks for the oxidation of acetaldehyde (CH_3CHO, 0.125 M), acetic acid (CH_3COOH, 0.125 M), and ethanol (CH_3CH_2OH, 0.125M) in a 0.1 M perchloric acid solution.

mixture of CO_2 and intermediates, such as acetaldehyde and acetic acid, would be more likely to form during the ethanol oxidation, since C−C bond cleavage remained a mechanistically difficult step.[58−65] Here we further studied the activity of $Pt_{95}Bi_5$ NW networks toward acetaldehyde and acetic acid oxidation (Figure 7). It clearly showed that $Pt_{95}Bi_5$ was only active toward the oxidation of acetaldehyde, in which two oxidation peaks appeared in the forward scan, analogous to that in ethanol oxidation. Our data indicated ethanol oxidation on Pt/Bi might occur through a formation of acetaldehyde (Pt·CH_3CHO) as an intermediate and acetic acid might be the major final product, which has also been reported in the Pt/C catalysts via various in situ measurements.[58,59,61−63,65−68]

It is also important to note that the synthesis and preparation conditions have not been optimized for Pt/Bi catalyst. The electrochemical measurements were conducted on as-made unsupported Pt/Bi, in sharp contrast to commercial Pt/C (ETEK), which has been extensively explored and optimized for fuel cell applications. Our catalysts, especially $Pt_{95}Bi_5$, still exhibit superior activity for ethanol oxidation even under these nonoptimized conditions. Thus, the enhanced activity from Pt/Bi can still be considered as a lower limit on the electrooxidation of ethanol.

Conclusion

In conclusion, dendrite-like Pt/Bi NW networks with a high aspect ratio were successfully synthesized through the Polyol approach by fine control over the synthetic conditions, such as the concentration of Bi species and reaction time. The formation mechanism of Pt/Bi NW networks was proposed and discussed with respect to the Bi-oriented anisotropic

attachment growth. The as-made $Pt_{95}Bi_5$ appeared to have superior electrocatalytic activity toward ethanol oxidation in comparison with commercial Pt/C. We believe our sophisticated experimental investigations and advanced characterization techniques, especially the aberration-corrected STEM and XANES techniques, combined with catalytic measurements, will complement each other and offer unique opportunities in the research on the ethanol fuel cell catalysts, which are substantial technology of growing interest and commercialization.

Acknowledgment. This work is supported in part by the University of New Hampshire (X.T., W.D.) and the U.S. Department of Energy (A.I.F., Q.W., Grant No. DE-FG02-03ER15476). Beamlines X19A/X18B are partly supported by Synchrotron Catalysis Consortium under contract DE-FG02-05ER15688.

Supporting Information Available: EDS and XRD spectra and TEM images of Pt/Bi nanostructures. This material is available free of charge via the Internet at http://pubs.acs.org.

References

(1) Parsons, R.; Vandernoot, T. *J. Electroanal. Chem.* **1988**, *257*, 9–45.
(2) Wasmus, S.; Kuver, A. *J. Electroanal. Chem.* **1999**, *461*, 14–31.
(3) Lamy, C.; Rousseau, S.; Belgsir, E. M.; Coutanceau, C.; Leger, J. M. *Electrochim. Acta* **2004**, *49*, 3901–3908.
(4) Antolini, E. *J. Power Sources* **2007**, *170*, 1–12.
(5) Ren, X. M.; Zelenay, P.; Thomas, S.; Davey, J.; Gottesfeld, S. *J. Power Sources* **2000**, *86*, 111–116.
(6) Xia, X. H.; Liess, H. D.; Iwasita, T. *J. Electroanal. Chem.* **1997**, *437*, 233–240.
(7) Xu, D.; Liu, Z.; Yang, H.; Liu, Q.; Zhang, J.; Fang, J.; Zou, S.; Sun, K. *Angew. Chem., Int. Ed.* **2009**, *48*, 1–6.
(8) Cremers, C.; Scholz, M.; Seliger, W.; Racz, A.; Knechtel, W.; Rittmayr, J.; Grafwallner, F.; Peller, H.; Stimming, U. *Fuel Cells* **2007**, *7*, 21–31.
(9) Iwasita, T. *Electrochim. Acta* **2002**, *47*, 3663–3674.
(10) Huber, G. W.; Iborra, S.; Corma, A. *Chem. Rev.* **2006**, *106*, 4044–4098.
(11) Lynd, L. R.; Cushman, J. H.; Nichols, R. J.; Wyman, C. E. *Science* **1991**, *251*, 1318–1323.
(12) Bardi, U. *Rep. Prog. Phys.* **1994**, *57*, 939–987.
(13) Gasteiger, H. A.; Markovic, N. M.; Ross, P. N. *J. Phys. Chem.* **1995**, *99*, 8290–8301.
(14) Chrzanowski, W.; Wieckowski, A. *Langmuir* **1998**, *14*, 1967–1970.
(15) Paulus, U. A.; Endruschat, U.; Feldmeyer, G. J.; Schmidt, T. J.; Bonnemann, H.; Behm, R. J. *J. Catal.* **2000**, *195*, 383–393.
(16) Teng, X. W.; Maksimuk, S.; Frommer, S.; Yang, H. *Chem. Mater.* **2007**, *19*, 36–41.
(17) Camara, G. A.; de Lima, R. B.; Iwasita, T. *Electrochem. Commun.* **2004**, *6*, 812–815.
(18) Campbell, S. A.; Parsons, R. *J. Chem. Soc.-Faraday Trans.* **1992**, *88*, 833–841.
(19) Schmidt, T. J.; Grgur, B. N.; Behm, R. J.; Markovic, N. M.; Ross, P. N. *Phys. Chem. Chem. Phys.* **2000**, *2*, 4379–4386.
(20) Schmidt, T. J.; Stamenkovic, V. R.; Lucas, C. A.; Markovic, N. M.; Ross, P. N. *Phys. Chem. Chem. Phys.* **2001**, *3*, 3879–3890.
(21) Tripkovic, A. V.; Popovic, K. D.; Stevanovic, R. M.; Socha, R.; Kowal, A. *Electrochem. Commun.* **2006**, *8*, 1492–1498.
(22) Xia, D. G.; Chen, G.; Wang, Z. Y.; Zhang, J. J.; Hui, S. Q.; Ghosh, D.; Wang, H. J. *Chem. Mater.* **2006**, *18*, 5746–5749.
(23) Wang, L. L.; Johnson, D. D. *J. Phys. Chem. C* **2008**, *112*, 8266–8275.
(24) Jeyabharathi, C.; Mathiyarasu, J.; Phani, K. L. N. *J. Appl. Electrochem.* **2009**, *39*, 45–53.
(25) Casado-Rivera, E.; Gal, Z.; Angelo, A. C. D.; Lind, C.; DiSalvo, F. J.; Abruna, H. D. *ChemPhysChem* **2003**, *4*, 193–199.
(26) Casado-Rivera, E.; Volpe, D. J.; Alden, L.; Lind, C.; Downie, C.; Vazquez-Alvarez, T.; Angelo, A. C. D.; DiSalvo, F. J.; Abruna, H. D. *J. Am. Chem. Soc.* **2004**, *126*, 4043–4049.
(27) Oana, M.; Hoffmann, R.; Abruna, H. D.; DiSalvo, F. J. *Surf. Sci.* **2005**, *574*, 1–16.
(28) Roychowdhury, C.; Matsumoto, F.; Mutolo, P. F.; Abruna, H. D.; DiSalvo, F. J. *Chem. Mater.* **2005**, *17*, 5871–5876.
(29) Blasini, D. R.; Rochefort, D.; Fachini, E.; Alden, L. R.; DiSalvo, F. J.; Cabrera, C. R.; Abruna, H. D. *Surf. Sci.* **2006**, *600*, 2670–2680.
(30) Roychowdhury, C.; Matsumoto, F.; Zeldovich, V. B.; Warren, S. C.; Mutolo, P. F.; Ballesteros, M.; Wiesner, U.; Abruna, H. D.; DiSalvo, F. J. *Chem. Mater.* **2006**, *18*, 3365–3372.
(31) Burda, C.; Chen, X. B.; Narayanan, R.; El-Sayed, M. A. *Chem. Rev.* **2005**, *105*, 1025–1102.
(32) Xiong, Y. J.; Wiley, B.; Xia, Y. N. *Angew. Chem.-Int. Ed.* **2007**, *46*, 7157–7159.
(33) Lee, E. P.; Peng, Z. M.; Chen, W.; Chen, S. W.; Yang, H.; Xia, Y. N. *ACS Nano* **2008**, *2*, 2167–2173.
(34) Lu, X. M.; Rycenga, M.; Skrabalak, S. E.; Wiley, B.; Xia, Y. N. *Annu. Rev. Phys. Chem.* **2009**, *60*, 167–192.
(35) Peng, Z. M.; Yang, H. *Nano Today* **2009**, *4*, 143–164.
(36) Tian, N.; Zhou, Z. Y.; Sun, S. G.; Ding, Y.; Wang, Z. L. *Science* **2007**, *316*, 732–735.
(37) Markovic, N. M.; Ross, P. N. *Surf. Sci. Rep.* **2002**, *45*, 121–229.
(38) Teng, X. W.; Liang, X. Y.; Maksimuk, S.; Yang, H. *Small* **2006**, *2*, 249–253.
(39) Lim, B.; Jiang, M.; Camargo, P. H. C.; Cho, E. C.; Tao, J.; Lu, X.; Zhu, Y.; Xia, Y. *Science* **2009**, *324*, 1302–1305.
(40) Peng, Z. M.; Yang, H. *J. Am. Chem. Soc.* **2009**, *131*, 7542-+.
(41) Solla-Gullon, J.; Vidal-Iglesias, F. J.; Lopez-Cudero, A.; Garnier, E.; Feliu, J. M.; Aldaza, A. *Phys. Chem. Chem. Phys.* **2008**, *10*, 3689–3698.
(42) Colmati, F.; Tremiliosi-Filho, G.; Gonzalez, E. R.; Berna, A.; Herrero, E.; Feliu, J. M. *Faraday Discuss.* **2008**, *140*, 379–397.
(43) Maksimuk, S.; Yang, S. C.; Peng, Z. M.; Yang, H. *J. Am. Chem. Soc.* **2007**, *129*, 8684-+.
(44) Yang, S. C.; Peng, Z. M.; Yang, H. *Adv. Funct. Mater.* **2008**, *18*, 2745–2753.
(45) Pennycook, S. J.; Varela, M.; Hetherington, C. J. D.; Kirkland, A. I. *MRS Bull.* **2006**, *31*, 36–43.
(46) Inada, H.; Wu, L. J.; Wall, J.; Su, D.; Zhu, Y. *J. Electron Microsc.* **2009**, *58*, 111–116.
(47) Tang, Z. Y.; Kotov, N. A. *Adv. Mater.* **2005**, *17*, 951–962.
(48) Tang, Z. Y.; Kotov, N. A.; Giersig, M. *Science* **2002**, *297*, 237–240.
(49) Song, Y.; Garcia, R. M.; Dorin, R. M.; Wang, H. R.; Qiu, Y.; Coker, E. N.; Steen, W. A.; Miller, J. E.; Shelnutt, J. A. *Nano Lett.* **2007**, *7*, 3650–3655.
(50) Teng, X. W.; Han, W. Q.; Ku, W.; Hucker, M. *Angew. Chem.-Int. Ed.* **2008**, *47*, 2055–2058.
(51) Xia, Y. N.; Yang, P. D.; Sun, Y. G.; Wu, Y. Y.; Mayers, B.; Gates, B.; Yin, Y. D.; Kim, F.; Yan, Y. Q. *Adv. Mater.* **2003**, *15*, 353–389.
(52) Wang, H.; Xu, C. W.; Cheng, F. L.; Jiang, S. P. *Electrochem. Commun.* **2007**, *9*, 1212–1216.
(53) Xu, C. W.; Wang, H.; Shen, P. K.; Jiang, S. P. *Adv. Mater.* **2007**, *19*, 4256–4260.
(54) Frenkel, A. I.; Hills, C. W.; Nuzzo, R. G. *J. Phys. Chem. B* **2001**, *105*, 12689–12703.
(55) Teng, X. W.; Han, W. Q.; Wang, Q.; Li, L.; Frenkel, A. I.; Yang, J. C. *J. Phys. Chem. C* **2008**, *112*, 14696–14701.
(56) Teng, X. W.; Feygenson, M.; Wang, Q.; He, J. Q.; Du, W. X.; Frenkel, A. I.; Han, W. Q.; Aronson, M. *Nano Lett.* **2009**, *9*, 3177–3184.
(57) Menard, L. D.; Gao, S. P.; Xu, H. P.; Twesten, R. D.; Harper, A. S.; Song, Y.; Wang, G. L.; Douglas, A. D.; Yang, J. C.; Frenkel, A. I.; Nuzzo, R. G.; Murray, R. W. *J. Phys. Chem. B* **2006**, *110*, 12874–12883.
(58) Lai, S. C. S.; Kleyn, S. E. F.; Rosca, V.; Koper, M. T. M. *J. Phys. Chem. C* **2008**, *112*, 19080–19087.
(59) Lai, S. C. S.; Koper, M. T. M. *Faraday Discuss.* **2008**, *140*, 399–416.
(60) Kowal, A.; Li, M.; Shao, M.; Sasaki, K.; Vukmirovic, M. B.; Zhang, J.; Marinkovic, N. S.; Liu, P.; Frenkel, A. I.; Adzic, R. R. *Nat. Mater.* **2009**, *8*, 325–330.
(61) Lai, S. C. S.; Koper, M. T. M. *Phys. Chem. Chem. Phys.* **2009**, *11*, 10446–10456.
(62) Wang, H.; Jusys, Z.; Behm, R. J. *J. Power Sources* **2006**, *154*, 351–359.
(63) Wang, Q.; Sun, G. Q.; Jiang, L. H.; Xin, Q.; Sun, S. G.; Jiang, Y. X.; Chen, S. P.; Jusys, Z.; Behm, R. J. *Phys. Chem. Chem. Phys.* **2007**, *9*, 2686–2696.
(64) Wang, H. S.; Alden, L.; DiSalvo, F. J.; Abruna, H. D. *Phys. Chem. Chem. Phys.* **2008**, *10*, 3739–3751.
(65) Camara, G. A.; Iwasita, T. *J. Electroanal. Chem.* **2005**, *578*, 315–321.
(66) Rao, V.; Cremers, C.; Stimming, U.; Cao, L.; Sun, S. G.; Yan, S. Y.; Sun, G. Q.; Xin, Q. *J. Electrochem. Soc.* **2007**, *154*, B1138–B1147.
(67) Rao, V.; Hariyanto; Cremers, C.; Stimming, U. *Fuel Cells* **2007**, *7*, 417–423.
(68) Iwasita, T.; Nart, F. C. *Prog. Surf. Sci.* **1997**, *55*, 271–340.